The Meteoritical Society

Meteoritics & Planetary Science 42, Nr 9, 1615–1625 (2007)
Abstract available online at http://meteoritics.org

Crater geometry and ejecta thickness of the Martian impact crater Tooting

Peter J. MOUGINIS-MARK and Harold GARBEIL

Hawai'i Institute of Geophysics and Planetology, University of Hawai'i, Honolulu, Hawai'i 96822, USA

(Received 25 October 2006; revision accepted 04 March 2007)

Abstract–We use Mars Orbiter Laser Altimeter (MOLA) topographic data and Thermal Emission Imaging System (THEMIS) visible (VIS) images to study the cavity and the ejecta blanket of a very fresh Martian impact crater ~29 km in diameter, with the provisional International Astronomical Union (IAU) name Tooting crater. This crater is very young, as demonstrated by the large depth/diameter ratio (0.065), impact melt preserved on the walls and floor, an extensive secondary crater field, and only 13 superposed impact craters (all 54 to 234 meters in diameter) on the ~8120 km^2 ejecta blanket. Because the pre-impact terrain was essentially flat, we can measure the volume of the crater cavity and ejecta deposits. Tooting crater has a rim height that has >500 m variation around the rim crest and a very large central peak (1052 m high and >9 km wide). Crater cavity volume (i.e., volume below the pre-impact terrain) is ~380 km^3 and the volume of materials above the pre-impact terrain is ~425 km^3. The ejecta thickness is often very thin (<20 m) throughout much of the ejecta blanket. There is a pronounced asymmetry in the ejecta blanket, suggestive of an oblique impact, which has resulted in up to ~100 m of additional ejecta thickness being deposited down-range compared to the up-range value at the same radial distance from the rim crest. Distal ramparts are 60 to 125 m high, comparable to the heights of ramparts measured at other multi-layered ejecta craters. Tooting crater serves as a fresh end-member for the large impact craters on Mars formed in volcanic materials, and as such may be useful for comparison to fresh craters in other target materials.

INTRODUCTION

Since the earliest days of the Viking Orbiter missions, analysis of the lobate deposits surrounding many Martian impact craters has suggested the presence of water or ice within the top kilometer or so of the crust at the time of crater formation (Carr et al. 1977; Gault and Greeley 1978; Mouginis-Mark 1979). The terms "rampart crater" and "multi-layered ejecta craters" have been used to describe these craters on Mars (Barlow et al. 2000). Impact craters on any planetary surface provide crucial information on the subsurface structure of the target material, as well as insights into the cratering process. In the case of Martian craters, the three-dimensional structure is particularly important as it may provide evidence for spatial or temporal variations in the distribution of subsurface volatiles. But due to the presence of these volatiles and an atmosphere (both of which increase the rate of modification of the crater), one particularly challenging task is to determine the original morphological attributes of fresh craters prior to their modification by erosion and/or deposition.

Using images from the Thermal Emission Imaging System (THEMIS) and the Mars Orbiter Camera (MOC), we have identified a 29 km diameter crater located at 23.4°N, 207.5°E that meets many of the criteria for having formed in the very recent past, perhaps within the last few million years (Mouginis-Mark et al. 2003). This crater, which has provisionally been given the name Tooting crater by the International Astronomical Union (after a town in southwestern London, England), lies to the west of the Olympus Mons aureole and formed in lava flows from the volcano (Fig. 1a). Tooting crater has been the target of numerous imaging opportunities by the THEMIS Science Team, providing almost complete coverage at a spatial resolution of 18 m/pixel (Fig. 2). Tooting crater is a multi-layered ejecta crater, based upon the classification of Barlow et al. (2000). Inspection of the 30 THEMIS VIS images of Tooting that have been collected by the end of 2006 (Fig. 2) reveals that there is a total of 13 superposed impact craters on the ejecta blanket, which has an area of ~8120 km^2. These craters have diameters ranging between 54 and 234 meters (equivalent to 3 to 13 THEMIS pixels). We binned the number of craters based upon their diameter, and for impacts superposed upon the Tooting crater ejecta blanket in the diameter range 88 to 125 meters, the crater density is ~0.00049 1/km^2 and for the craters in the diameter range 125

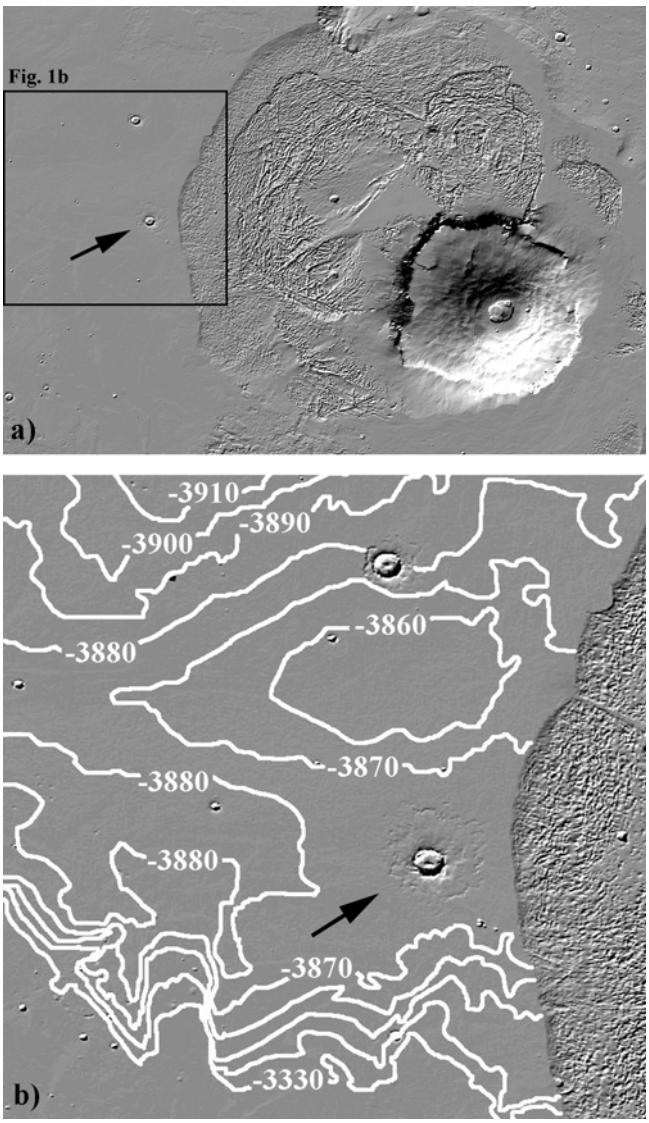

Fig. 1. a) Location map for Tooting crater (arrowed), which lies just to the west of the Olympus Mons aureole at 23.4°N, 207.5°E. Base image is a MOLA shaded relief version of the topographic data set from 10°–35°N, 200°–235°E. The black rectangle outlines the area shown in (b). b) Topography of the area surrounding Tooting crater (arrowed), derived from the MOLA 128th degree DEM. Contours are at 10-meter intervals and provide elevations relative to the Mars datum. Note that the contours for the Olympus Mons aureole materials have been omitted for clarity. Base image is a MOLA shaded relief image.

to 176 m the crater density is ~0.00074. Using the final 2004 iteration of the Martian crater-count isochron (see Table 2 in Hartmann 2005), this gives an approximate age for Tooting crater that is most likely less than 2 Myr, and is probably in the range of 0.4 to 1.7 Myr. Our analysis of this morphologically fresh crater not only provides information on the original geometry of large impact craters on Mars, but also enables the original morphology of the crater cavity and ejecta layers to be examined. In addition, it places constraints on the recent subsurface distribution of volatiles, and because of the relatively young volcanic target rocks (Scott and Tanaka 1986; Fuller and Head 2002) has potential implications for the source area of at least some of the basaltic SNC meteorites and the petrologic interpretation of these rocks (Mouginis-Mark et al. 1992; McSween et al. 1996; Kring et al. 2003).

Tooting crater formed on virtually flat lava flows within Amazonis Planitia (Fig. 1b) where there appear to have been no other major topographic features prior to the impact. The crater formed in a flat area ~185 × 135 km in size that is at an elevation between –3870 m and –3880 m relative to the Mars datum. Locally, just beyond the ramparts of the ejecta layers in all azimuths, the elevation varies from –3870 m to –3874 m. The depth of the crater and the thickness of the ejecta blanket can therefore be determined by subtracting the appropriate elevation of the surrounding landscape (–3872 m) from the individual MOLA measurements. Thus, for the first time, it is possible to determine the absolute ejecta thicknesses for a fresh multi-layered impact crater on Mars as the radial decrease of thickness as a function of distance away from the rim crest. It is also possible to study the geometry of this fresh large crater using the MOLA measurements. As such, this study serves as a reference point against which to study the ejecta of more eroded multi-layered ejecta craters of similar size; knowledge of the radial distribution of ejecta for craters in the southern highlands may be particularly important for assessing erosion rates of craters at different periods of the history of Mars (Forsberg-Taylor et al. 2004). Tooting crater may also serve as reference point against which to compare the geometry of fresh craters of similar size that formed in other target materials such as the northern plains (Boyce and Mouginis-Mark 2006), where double-layered ejecta craters are far more common than on young lava flows such as those found in Amazonis Planitia (Barlow and Perez 2003).

CRATER CAVITY GEOMETRY

Thirty-two Mars Orbiter Laser Altimeter (MOLA) orbits cross the rim crest of Tooting crater (Fig. 3), permitting a profile around the rim crest of the crater to be determined. Figure 4 shows the location of the measured points and the variation in height around the rim crest using the individual MOLA shots. These measurements were obtained by using each individual MOLA profile that crosses the rim crest, and by identifying the highest point within each profile where it crosses the rim crest. We choose to use this shot-by-shot method for the identification of the rim height, rather than using the interpolated 128th-degree MOLA digital elevation model (DEM), because our measurements avoid using interpolated data in the DEM that might either include MOLA shots that are not the highest points on the rim, or include interpolated data between MOLA profiles. The spacing of our rim height measurements is therefore not uniform because the

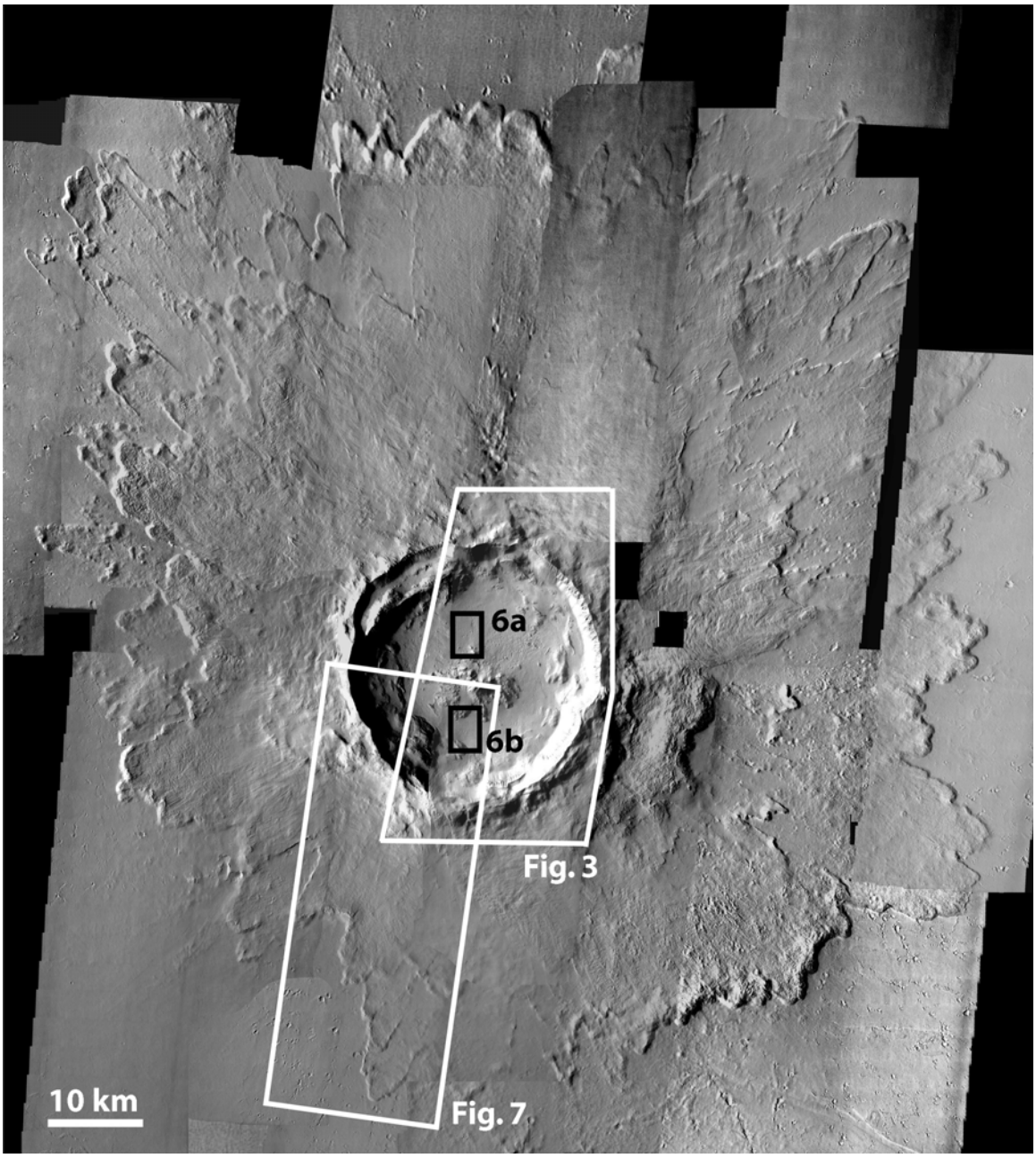

Fig. 2. Mosaic of THEMIS VIS images of Tooting crater. Outlined areas show the coverage of Figs. 3, 6, and 7. The black arrow at lower left indicates the direction of impact for the projectile that produced Tooting crater, as inferred from the asymmetry of the ejecta blanket. North is towards the top of the figure. Mosaic of THEMIS images V01965003, V01990003, V05710012, V09879009, V09904026, V10528009, V10815008, V10840007, V11127008, V111526006, V11439007, V11464014, V12063004, V12350008, V12662009, V13286006, V13573002, V13598009, V13885011, V16955013, V17579021, V17866018, V17891012, V18178024, V18203021, V18802011, V19114009, V19738008, V20050003, and V20986002.

location of each MOLA profile is non-uniform (Zuber et al. 1992). The distances along the rim profile (Fig. 4b) represent the straight-line distance between these high points for each profile. We caution, however, that these rim height measurements are limited by the precise location of the individual MOLA shots, and the finite size of the laser footprint (~140 m; Zuber et al. 1992; Stewart and Valiant 2006). It is therefore possible that higher points along each profile may have been averaged with lower parts of the rim (either the upper inner wall of the cavity or lower segments of the outer rim) to produce a lower MOLA-measured elevation. It is also likely that higher parts of the rim crest were not measured at all because of the absence of a MOLA ground-track.

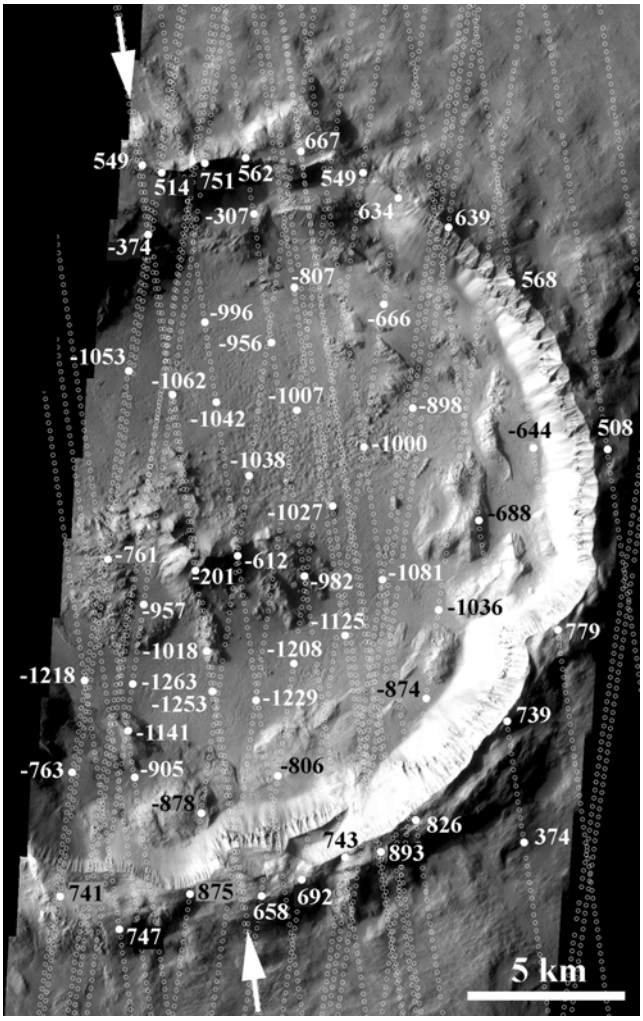

Fig. 3. Distribution of heights (in meters, relative to the –3872 m datum of the surrounding landscape) within the cavity of Tooting crater. The elevations at the rim crest are the values used for the construction of the rim profile in Fig. 4. Individual MOLA shots are shown as open white circles. The pair of white arrows denotes the location of the cross section through the crater that is displayed in Fig. 5. See Fig. 2 for location of this subscene of the cavity. THEMIS image V12662009.

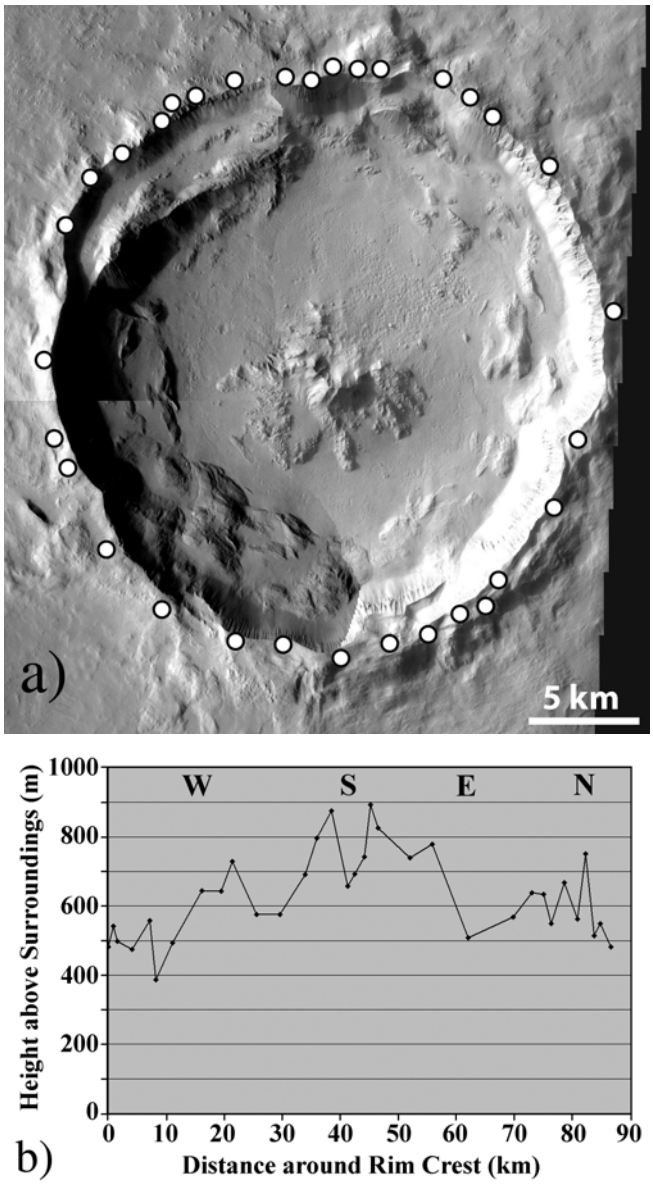

Fig. 4. Profile around the rim crest of Tooting crater. a) Location of the 32 points that can be measured around the rim using individual MOLA shots. North is toward the top of the image. b) The rim height as a function of distance around the rim crest, using the points identified in Fig. 4a. The height values are calculated relative to the –3872 m datum. The distance along the profile represents the straight-line distance between these points, and as such has an irregular spacing due to the precise location of each MOLA profile. The approximate compass bearings are given at the top of the profile. Vertical exaggeration is ×50.

The measured rim crest has a minimum height of 386 m above the surrounding terrain, a maximum height of 893 m, and an average height of 628 m. Taking 29 km as the diameter of Tooting crater, the average value gives a rim height/crater diameter ratio of 0.022. The rim profile indicates that the southern rim has the highest elevations and that the northwestern rim has the lowest values. Inspection of Fig. 2 illustrates that the maximum range of the ejecta layers is generally greatest to the north and smallest to the south, suggesting an inverse relationship between ejecta range and rim height. We will return to this observation in the section on the distribution of the ejecta.

Geometric data can also be determined for the interior of the crater cavity. Figure 5 presents the profile (MOLA orbit 16,525) that crosses the highest point of the central peak complex and that coincidentally also crosses the lowest measured point of the crater floor. Although higher points on the central peak and lower points on the floor may exist, these values are the greatest measured by MOLA. A total of 14 individual MOLA profiles cross the central peak complex, enabling the geometry of the complex to be determined. The

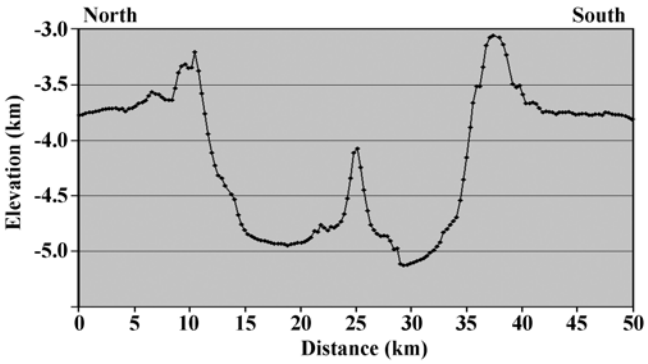

Fig. 5. Topographic profile taken through the highest point on central peak of Tooting crater. Profile derived from MOLA orbit 14,387. See Fig. 3 for location. Vertical exaggeration is ×10.

highest point of the central peak is at an elevation of –4073 m relative to the datum. From other MOLA profiles, there is a secondary peak that attains an elevation of –4484 m (orbit 14,387), a broad low rise to the west of the main central peak that reaches an elevation of –4633 m (orbit 11,840), and a smaller rise to the east of the central peak reaches –4641 m (orbit 19,196). The lowest elevation of the southern crater floor is –5125 m (orbit 16,525), as measured from 24 MOLA orbits that cross this part of the crater. The lowest elevation of the northern crater floor is –4934 m (orbit 16,525), as measured from 26 MOLA orbits.

Thus, the maximum height of the central peak above the northern floor is 861 m, and the maximum height of the central peak above the southern floor is 1052 m. Central peak width is 9828 m (E-W) and 8280 m (N-S), giving an average width of 9054 m. The average height-to-base ratio of the central peak is 0.106. The central peak width is appreciably larger than the 6065 m predicted by the relationships developed by Hale (1983) for 1672 Martian craters, and lies at the +1 sigma value for craters with the diameter of Tooting crater.

The measured depth below average rim crest is 1690 m for northern floor, and 1881 m for southern floor. Garvin and Frawley (1998) established the relationship $d = 0.25\ D^{0.49}$, where d is the depth and D the diameter, both in kilometers, for 98 of the most unmodified Martian craters. Using this relationship, Tooting crater should have a depth of 1302 m, but in reality it is ~1.3 times deeper on the northern floor, and ~1.4 times deeper on the southern floor, than predicted by Garvin and Frawley (1998) for this diameter.

The large depth and large central peak width suggest that Tooting crater may have significantly less infill material than is typical for Martian craters of this diameter. This interpretation is also supported from analysis of MOC images of the floor (Fig. 6), which reveals that the southern floor has a polygonally fractured surface similar in morphology to the impact melt identified in lunar craters such as Tycho and Aristarchus (Strom and Fielder 1971), Copernicus (Howard and Wilshire 1975) and King (Heather and Dunkin 2003). The northern floor appears to be more mantled, with many pits that are a few hundreds of meters in diameter on the floor (Fig. 6a), suggesting that some other type of material (the origin of which is as yet unidentified) may lie on top of an impact melt sheet.

EJECTA DISTRIBUTION

The ejecta deposits around multi-layered ejecta craters are thought to be closely tied to target properties and the ambient conditions at the time of impact. Typically, this has been attributed to the presence of volatiles (water or ice) within the target material at the time of crater formation (Carr et al. 1977; Gault and Greeley 1978; Mouginis-Mark 1979). Alternative models attributing atmospheric effects have also been proposed (e.g., Schultz and Gault 1979; Schultz 1992; Barnouin-Jha and Schultz 1998). In the case of Tooting crater, the ejecta deposit is asymmetric (Fig. 2). Presumably, this asymmetry is due to the angle of impact of the projectile that formed the crater, as there is no topographic gradient in the vicinity of Tooting crater (Fig. 1b) that could have influenced gravity-driven flow of the ejecta (Mouginis-Mark and Baloga 2006).

Few previous studies have investigated the thickness of these ejecta deposits, but the radial decay of thickness most likely is directly relevant to the emplacement process (Baloga et al. 2005; Barnouin-Jha et al. 2005; Mouginis-Mark and Baloga 2006). Once more assuming a flat pre-impact surface and a base elevation for the surrounding terrain of –3872 m relative to the MOLA data allows the spatial distribution of the thickness of the Tooting crater ejecta blanket to be explored. Point-by-point studies of the thickness of the ejecta reveals some surprising features of the Tooting crater ejecta blanket. For example, south of the crater rim (Fig. 7) the ejecta layers can be remarkably thin; there are places where the ejecta layers are between 3 to 5 m thick at radial distances of ~11 km from the rim crest, or ~30% of the maximum radial distance in that azimuth from the crater rim. Distal ramparts are 60–125 m high, comparable to the heights of ramparts measured at other multi-layered ejecta craters (Mouginis-Mark and Baloga 2006).

A total of 24,201 MOLA shots from 90 individual orbits lie on the ejecta blanket beyond the rim crest of Tooting crater out to a radial distance of 66.5 km (Fig. 8). The gridded 128th-degree MOLA elevation data show that the crater cavity volume (i.e., the volume of the cavity which lies below the –3872 m datum) is ~380 km^3 and the volume of materials above the elevation of the –3872 datum is ~425 km^3. Assuming no losses in the ejecta volume due to erosion, this implies that the amount of structural uplift of pre-existing strata (which is most important within ~0.8 to 1.2 crater radii from the rim crest; see p. 87 of Melosh 1989), and the bulking of the material that now forms the ejecta blanket,

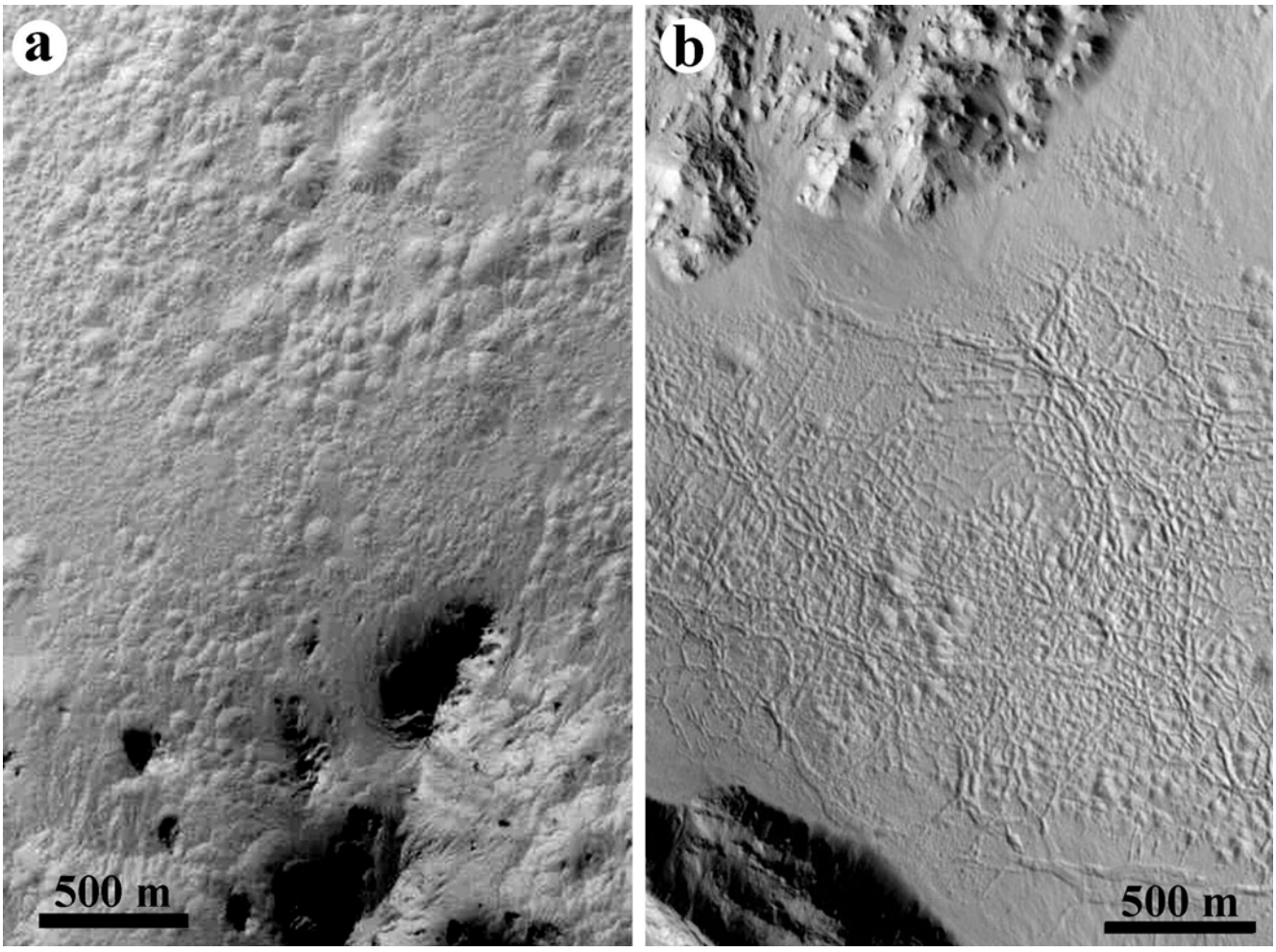

Fig. 6. A pair of MOC images showing the contrasting morphology of crater floor a) to the north and b) to the south of the central peak. The northern floor is hummocky with numerous pits (as yet of unknown origin), but no fractures on the floor. The southern floor has numerous polygonal cracks that are similar to the fractures seen within impact melt sheets on the Moon. See Fig. 2 for locations. Left image is S0900514 at 4.77 m/pixel. Right image is E0500856 at 4.53 m/pixel.

amounts to ~11.8% of all of the observed volume of the ejecta. This is within the range of the larger population of fresh Martian craters studied by Garvin and Frawley (1998), although they found that for craters ~30 km in diameter the ratio of ejecta volume to cavity volume was in the range 3.1 to >10. As noted by Garvin and Frawley (1998), this may be due to a partial infilling of the crater cavity with increasing age.

We have also studied the decrease of ejecta thickness at Tooting crater as a function of radial distance from the rim. It is apparent from Fig. 2 that Tooting crater formed as the result of an oblique impact, with the projectile coming from the southwest. In Fig. 9 we compare the radial distance of the ejecta layer from the rim crest with the azimuth angle, centered upon the central peak of Tooting crater, using azimuthal segments of 15°. For azimuths close to 210° (i.e., between 202.5° and 217.5°), which is the inferred up-range direction, the ejecta range is ~40 km. For the down-range direction (22.5° to 37.5°) the ejecta range is ~75–82 km. It is also possible to investigate the change in elevation (and hence in the thickness of the ejecta blanket) as a function of radial distance from the rim crest from the crater center (Fig. 10). Again, we use the raw MOLA data in this plot, rather than the gridded 128th-degree MOLA DEM, in order to avoid any interpolation of elevation measurements over topographic highs or lows. For the 15° azimuth sectors, we take the radial distance of each raw MOLA measurement from the rim crest (Fig. 4a). For each of these height measurements, we subtract the base elevation of –3872 m from the MOLA measurement, and bin the resultant thicknesses into 1.0 km increments. The sample size varies from 13 data points between 0 to 1.0 km from the rim crest to a maximum of 27 points between 32.0 to 33.0.

The contrast between the radial decay of ejecta thickness between the up-range and down-range azimuths is evident in Fig. 10, and the cross-range thicknesses are seen to be of intermediate values. For all azimuths, ejecta thicknesses are in excess of 400 m within 5 km of the rim crest. The greatest

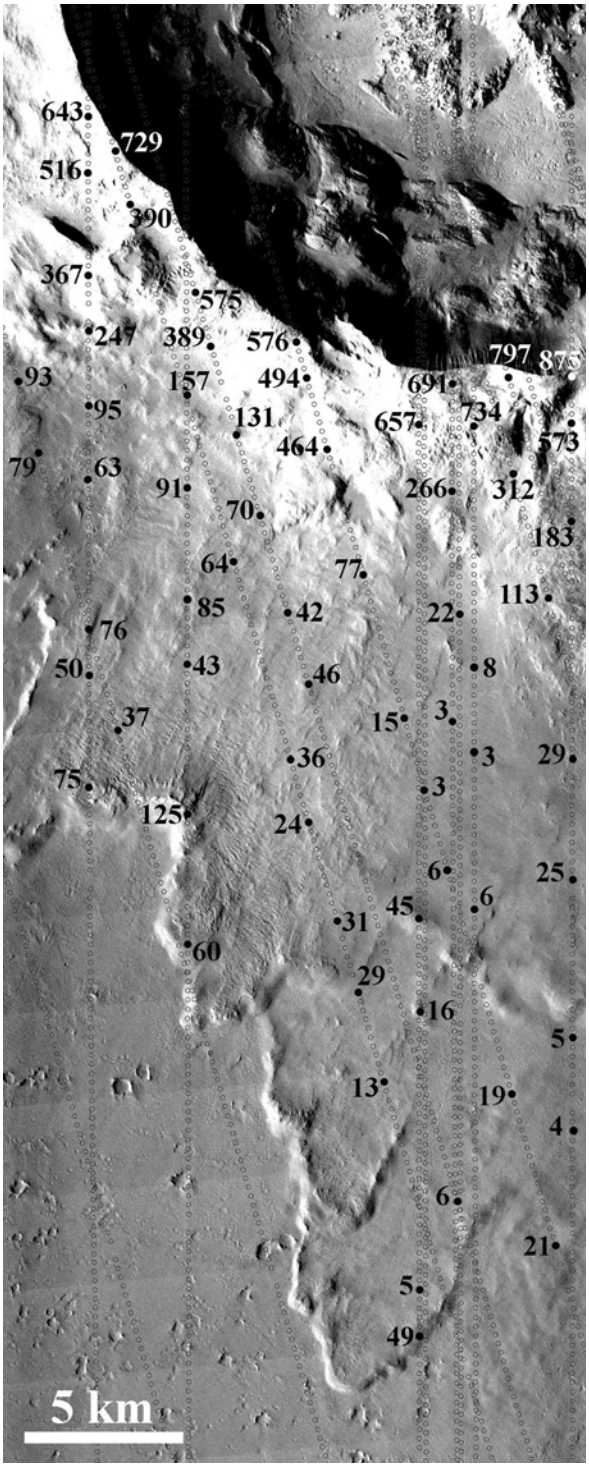

Fig. 7. Because Tooting crater formed on a surface that appears to have been flat and featureless, it is possible to measure the actual ejecta thickness at individual places using MOLA elevation data. Grey open circles show the individual MOLA shots. Here we give the ejecta thickness in meters, assuming that the base elevation is at –3872 m relative to the MOLA datum. Note that the thickness of the ejecta layer close to the distal rampart can be remarkably thin, often less than 10 m. The highest point on the crater rim is 875 m above the surrounding plain. See Fig. 2 for location. THEMIS image V01990003.

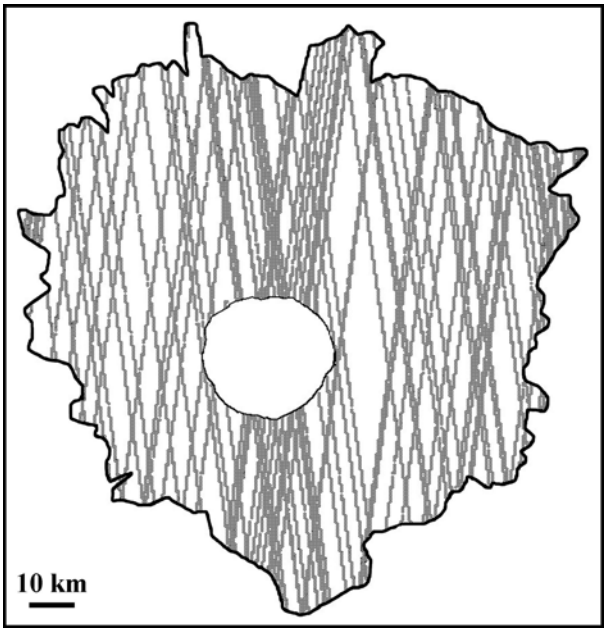

Fig. 8. Distribution of all MOLA shots that fall on the ejecta layers of Tooting crater. Over 90 individual MOLA profiles cross at least part of the ejecta blanket, and there are 24,201 individual elevation measurements on the ejecta blanket. The field of view is the same as that in Fig. 2.

difference between the up-range and down-range ejecta thicknesses occur at ~20 km from the rim crest, with an additional ~100 m of ejecta being deposited down-range compared to the up-range direction. At radial distances greater than ~65 km from the rim crest, there appears to be little difference in the down-range and cross-range ejecta thicknesses.

Mouginis-Mark and Baloga (2006) investigated the role of crater rim height in controlling the run-out distance of the ejecta in that azimuth direction. Figure 11 illustrates the relationship for Tooting crater using the same format of data presentation used by Mouginis-Mark and Baloga (2006) for ease of comparison of different craters on Mars. An interesting feature of Tooting crater is revealed in Fig. 11, namely that the ejecta have, in general, the largest run-out distances in azimuths where the rim height of the parent crater is low. This is contrary to the trends at two smaller multi-layered ejecta craters that Mouginis-Mark and Baloga (2006; their Fig. 11a) studied. For Toconao crater (21°S, 285°E), ejecta associated with the highest parts of the rim crest produced the greatest run-out distances. However, for both Toconao (diameter 17.9 km) and a crater within Chryse Planitia (16.0 km diameter, located at 28.4°N, 319.6°E), the maximum run-out distance is <3.0 crater radii. For Tooting crater, the maximum distance is ~4.0 crater radii. This difference may either be the result of the larger size of Tooting crater, or the fact that the oblique impact ejected material to a greater radial distance than was achieved by the (potentially) more vertical impacts associated with the other two craters.

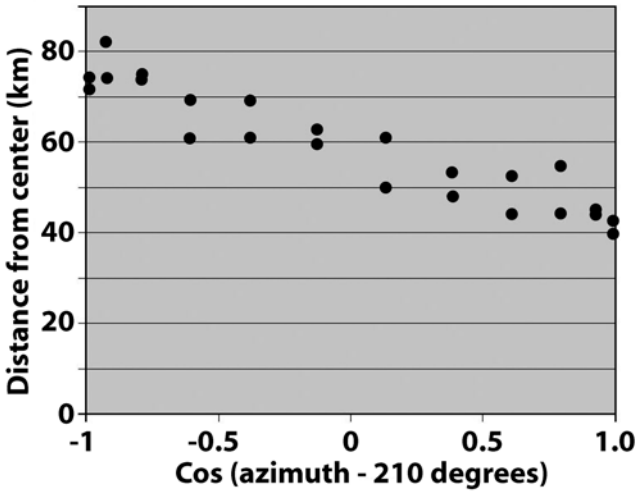

Fig. 9. The asymmetry of the ejecta blanket of Tooting crater is interpreted to be due to an oblique impact. This asymmetry can best be illustrated by plotting the maximum radial distance of the outer ejecta layer (taking the whole 15° sector) versus the cosine of the azimuth angle relative to the 210° azimuth. In this instance, the projectile is interpreted to have come from the southwest, so that the smallest radial distance is at this azimuth and the greatest radial distance is in the diametrically opposite direction (i.e., an azimuth of 30°).

DISCUSSION

Our ability to study the geometry of a large, young, multi-layered ejecta crater provides valuable insights into the cratering process on Mars. For example, the large central peak and the occurrence of impact-melt sheets at Tooting crater are rare features when compared to most Martian craters. The identification of impact melt within any large crater on Mars is of potential significance because impact melt has rarely been identified within impact craters on Mars. Indeed, the possible occurrence of volatiles within the target at the time of crater formation, as suggested by the fluidized ejecta deposits around the crater, has been predicted to preferentially destroy melt during the cratering process (Kieffer and Simonds 1980), although field analysis of Haughton crater by Osinski (2006) appears to support the idea of melt being generated in volatile-rich targets. Our observations of melt deposits within Tooting crater (Fig. 6) suggest that extensive melt sheets were created in this case, and allow us to speculate that impact melt may now be buried under sedimentary deposits within other craters on Mars. This observation supports the idea that hydrothermal systems may have once existed within some large craters that became flooded with water soon after their formation because of the large volume of (relatively) hot rock that could have persisted on the crater floor for extended periods of time (Newsom et al. 2001; Rathbun and Squyres 2002), perhaps as much as ~70,000 years (Abramov and Kring 2005).

The morphology of Tooting crater demonstrates that the fresh cavity of a multi-layered crater on Mars can be quite similar to fresh lunar craters such as Tycho and King craters. MOLA elevation data suggest that the central peak of Tooting crater is large only because of the small volume of infilling. If the floor was at an elevation of ~200 m below the mean datum, or ~830 m below the average rim height, then the central peak would be entirely buried. Thus, if Tooting crater was an older, more degraded, crater with a depth/diameter ratio of ~0.03, then the peak would be entirely buried. Furthermore, infilling the southern floor of the crater cavity with only ~200 m of material (thereby creating a crater with a depth/diameter ratio of 0.06) would bury all evidence of impact melt on the crater floor.

The observation that the majority of the ejecta layers are very thin at all azimuth angles at radial distances in excess of ~10 km from the rim of Tooting crater (Fig. 7) is striking and has implications for the mode of emplacement of ejecta on Mars. Mouginis-Mark and Baloga (2006) discussed the possibility that the distal ramparts that surround multi-layered ejecta craters such as Tooting contain the bulk of material that flowed across the surface as the ejecta layers formed. Most of the craters that Mouginis-Mark and Baloga (2006) were able to measure are located on tilted surfaces or formed in cratered landscapes that precluded the precise measurement of the actual thickness of the ejecta. They discovered that the ramparts may be as high as 180 m and as wide as 2.5 km.

Furthermore, there does not seem to be any consistent thickness for individual ejecta layers that would aid the interpretation of the mode of formation of the ejecta layers. For instance, we do not see any systematic thickening of a set of ejecta layers compared to individual layer variations. Inspection of Fig. 7 shows that close to the distal rampart, the ejecta layer is ~5–6 m thick. Moving toward the parent crater, and crossing two additional ramparts associated with other ejecta layers, results in an ejecta blanket that is still only 3 to 8 m in total thickness. The implication for ejecta emplacement appears to be that the ejecta blankets of multi-layered craters did not form in a manner that included stratigraphically higher layers being emplaced on top of early, more extensive layers. An inference from the preliminary measurements of fluidized craters by Mouginis-Mark and Baloga (2006) that basal erosion and horizontal movement of the substrate took place, in a comparable manner to that identified at Ries crater, Germany (Hörz et al. 1983; Kenkmann and Schonian 2006), may have taken place on Mars. Our measurements of Tooting crater show that there is little bulking of the ejecta layer with increasing radial distance (indeed, the opposite trend is identified in Fig. 10), so that the passive passage of the ejecta layer over the substrate may have been more common and that the final ejecta layer that can now be mapped from THEMIS images is remarkably thin except where the distal ramparts have formed. The thinness of the ejecta layers at Tooting crater, if they are typical for other impact craters on Mars, also

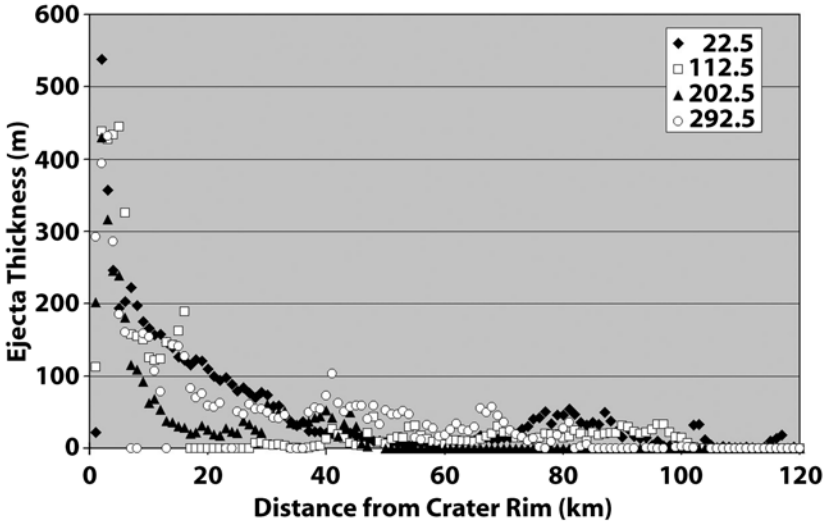

Fig. 10. Thickness of Tooting ejecta as a function of radial distance from the crater rim crest for the four principal azimuth directions, each covering a sector of 15°, corresponding to directly down-range (the 22.5° angle covers the range 15° to 30°), up-range (202.5° includes data from 195° to 210°), and cross-range (centered at 112.5° and 292.5°). Ejecta thickness has been determined by subtracting –3872 m from each of the MOLA measurements. Data average all measurements within a 15° sector centered on these azimuths, and are binned in 500 m intervals away from the crater rim crest. The total number of data points in this plot is ~24,200.

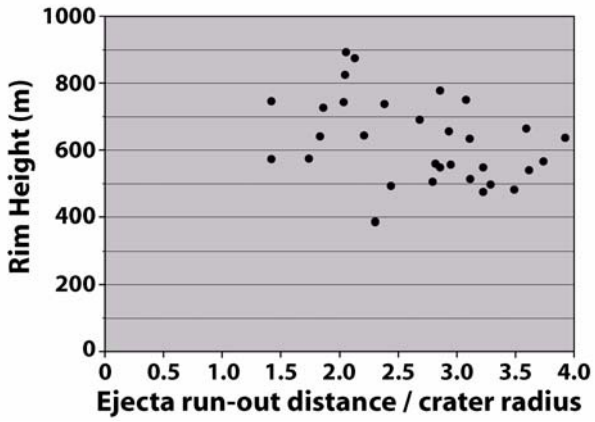

Fig. 11. Run-out distance, normalized to the radius of Tooting crater, compared to the rim height for that azimuth. Note the lack of large run-out distances for the highest parts of the rim. The rim height values are calculated relative to the local base level of –3872 m relative to the MOLA datum.

provides a supporting explanation for the observation that these materials could be easily diverted by pre-existing obstacles that might be several hundred meters to a kilometer in height (Baloga et al. 2005).

The azimuthal variation in rim height at Tooting crater is >500 m (Fig. 4), which brings into question the value of using rim height as a reference level to measure crater depth, and for developing a single rim height to diameter ratio for impact craters on Mars. The azimuthal variation in rim height of Tooting crater demonstrates that significantly different values (by as much as 500 m) could have been derived from the technique of De Hon (1981). This would be significant at other, older, craters for estimating the thickness of the surrounding lava flows depending upon where the rim height might have been measured using shadow length data. Estimations of erosion rates have also utilized the height of a crater rim. Arvidson et al. (1979) inspected Viking Lander images of craters seen in profile at the two lander sites to infer the degree of erosion, but there was insufficient information to measure the azimuthal variation in rim height for the craters imaged. In contrast, Forsberg-Taylor et al. (2004) employed the average rim height of an impact crater as the starting point of their assessment of the degree of modification of the landform either by fluvial or aeolian processes. Both approaches (i.e., a single measure of height or an approximation to the average rim height) make certain assumptions about pristine crater geometry. At Tooting crater, where we are confident that the crater is still fresh, we can quantify the azimuthal variation in rim height. It is also apparent at Tooting crater that different parts of the floor may have different elevations immediately after the crater formed; it seems probable that such height variations would be the first attribute of the floor to be modified by infilling as the lowest points on the floor would act as traps for eolian material, but these low points represent a much smaller area of the crater floor than would be predicted from the diameter of the crater. The freshest, least modified, craters on Mars may therefore be the ones that have primary floor structures at different elevations.

A key attribute of Tooting crater is that it formed in a flat, morphologically bland, part of Amazonis Planitia, which has a series of relatively young lava flows at the surface (Scott and Tanaka 1986; Fuller and Head 2002). Because of this flat terrain, we can confidently measure the geometry and thickness of the ejecta blanket to the spatial resolution of the MOLA data set. Tooting crater can therefore be taken as an end-member example of a fresh multi-layered ejecta

crater formed in lava flows. Future studies of Martian craters should search for comparable-sized craters that formed in other target materials (e.g., the hilly and cratered terrain of the southern highlands; Scott and Tanaka 1986) or at different latitudes and elevations (Mouginis-Mark 1979) so that the role of target properties in controlling crater geometry can be investigated (Stewart and Valiant 2006). Any improvement in the quality of topographic data for the crater will also enable the spatial distribution of ejecta thickness and the original radial decay of ejecta thickness from the rim crest to be refined. Such an opportunity will present itself with the acquisition of higher resolution topographic data from stereo images obtained from the High Resolution Imaging Science Experiment (HiRISE) onboard the Mars Reconnaissance Orbiter spacecraft. HiRISE is just now entering the data collection phase of the mission, and promises to bring further improvements in our knowledge of impact craters on Mars.

Acknowledgments–This work was supported in part by NASA grant NNX06AC61G from NASA's Planetary Geology and Geophysics Program. Steve Baloga provided comments on an earlier version of the manuscript. The review by Boris Ivanov was particularly helpful in stimulating our thinking on the asymmetric distribution of the ejecta. Nadine Barlow also provided a helpful review and several informative references. We thank Phil Christensen and the THEMIS Science Team, especially Laurel Cherednik, Kelly Bender, and Abdreas Dombovari, who were responsible for the targeting of THEMIS instrument to collect the near-complete coverage of Tooting crater, and to the creators of the THEMIS web site that facilitated our access to these data. Mike Malin and Ken Edgett are thanked for specifically targeting the MOC instrument to obtain the image in Fig. 6a under the MOC Public Target Request Program. This is HIGP Publication no. 1498 and SOEST Contribution no. 7168.

Editorial Handling—Dr. Elisabetta Pierazzo

REFERENCES

Abramov O. and Kring D. A. 2005. Impact-induced hydrothermal activity on early Mars. *Journal of Geophysical Research* 110: E12 S09, doi:10.1029/2005JE002453.

Arvidson R. E., Guiness E. A., and Lee S. 1979. Differential aeolian redistribution rates on Mars. *Nature* 278:533–535.

Baloga, S. M., Fagents S. A., and Mouginis-Mark P. J. 2005. Emplacement of Martian rampart crater deposits. *Journal of Geophysical Research* 110:E10 001, doi:10.1029/2004JE002338.

Barlow N. G., Boyce J. M., Costard F. M., Craddock R. A., Garvin J. B., Sakimoto S. E. H., Kuzmin R. O., Roddy D. J., and Soderblom L. A. 2000. Standardizing the nomenclature of Martian impact crater ejecta morphologies. *Journal of Geophysical Research* 105:26,733–26,738.

Barlow N. G. and Perez C. B. 2003. Martian impact crater ejecta morphologies as indicators of the distribution of subsurface volatiles. *Journal of Geophysical Research* 108:E8 5085, doi: 10.1029/2002JE002036.

Barnouin-Jha O. S. and Schultz P. H. 1998. Lobateness of impact ejecta deposits from atmospheric interactions. *Journal of Geophysical Research* 103:25,739–25,756.

Barnouin-Jha O. S., Baloga S., and Glaze L. 2005. Comparing landslides to fluidized crater ejecta on Mars. *Journal of Geophysical Research* 110:E04010, doi:10.1029/2003JE002214.

Boyce J. M. and Mouginis-Mark P. J. 2006. Martian craters viewed by the Thermal Emission Imaging System instrument: Double-layered ejecta craters. *Journal of Geophysical Research* 111:E10 005, doi:10.1029/2005JE002638.

Carr M. H., Crumpler L. S., Cutts J. A., Greeley R., Guest J. E., and Masursky H. 1977. Martian impact craters and emplacement of ejecta by surface flow. *Journal of Geophysical Research* 82: 4055–4065.

De Hon R. A. 1981. Thickness of volcanic materials on the east flank of the Tharsis plateau (abstract). Third International Colloquium on Mars. LPI Contribution #441. pp. 59– 61.

Forsberg-Taylor N. K., Howard A. D., and Craddock R. A. 2004. Crater degradation in the Martian highlands: Morphometric analysis of the Sinus Sabaeus region and simulation modeling suggest fluvial processes. *Journal of Geophysical Research* 109: E05002, doi:10.1029/2004JE002242.

Fuller E. R. and Head J. W. 2002. Amazonis Planitia: The role of geologically recent volcanism and sedimentation in the formation of the smoothest plains on Mars. *Journal of Geophysical Research* 107:E10, doi:10/1029/2002JE001842.

Garvin J. B., and Frawley J. J. 1998. Geometric properties of Martian impact craters: Preliminary results from Mars Orbiter Laser Altimeter. *Geophysical Research Letters* 25:4405–4408.

Gault D. E. and Greeley R. 1978. Exploratory experiments of impact craters formed in viscous-liquid targets: Analogs for Martian rampart craters? *Icarus* 34:486–495.

Hale W. S. 1983. Central structures in Martian impact craters: Morphology, morphometry, and implications for substrate volatile distribution (abstract). 14th Lunar and Planetary Science Conference. pp. 273–274.

Hartmann W. K. 2005. Martian cratering 8: Isochron refinement and the chronology of Mars. *Icarus* 174:294–320.

Heather D. J. and Dunkin S. K. 2003. Geology and stratigraphy of King crater, lunar far side. *Icarus* 163:307–329.

Hörz F., Ostertag R., and Rainey D. A. 1983. Bunte breccia of Ries: Continuous deposits of large impact craters. *Reviews of Geophysics and Space Physics* 21:1667–1725.

Howard K. A. and Wilshire H. G. 1975. Flows of impact melt at lunar craters. *U.S. Geological Survey Journal of Research* 3:237–251.

Kenkmann T. and Schonian F. 2006. Ries and Chicxulub: Impact craters on Earth provide insights for Martian ejecta blankets. *Meteoritics & Planetary Science* 41:1587–1603.

Kieffer S. W. and Simonds C. H. 1980. The role of volatiles and lithology in the impact cratering process. *Reviews of Geophysics and Space Physics* 18:143–181.

Kring D. A., Gleason J. D., Swindle T. D., Nishiizumi K., Caffee M. W., Hill D. H., Jull A. J. T., and Boynton W. V. 2003. Composition of the first bulk melt sample from a volcanic region of Mars: Queen Alexandra Range 94201. *Meteoritics & Planetary Science* 38:1833–1848.

McSween H. Y., Eisenhour D. D., Taylor L. A., Wadhwa M., and Crozaz G. 1996. QUE 94201 shergottite: Crystallization of a Martian basaltic magma. *Geochimica et Cosmochimica Acta* 60: 4563–4569.

Melosh H. J. 1989. *Impact cratering: A geological process*. New York: Oxford University Press. 245 p.

Mouginis-Mark P. J. 1979. Martian fluidized crater morphology: Variations with crater size, latitude, altitude, and target material. *Journal of Geophysical Research* 84:8011–8022.

Mouginis-Mark P. J. and Baloga S. M. 2006. Morphology and geometry of the distal ramparts of Martian impact craters. *Meteoritics & Planetary Science* 41:1469–1482.

Mouginis-Mark P. J., Boyce J. M., Hamilton V. E., Anderson F. S. 2003. A very young, large, impact crater on Mars. Sixth International Mars Conference (abstract #3004). CD-ROM.

Mouginis-Mark P. J., McCoy T. J., Taylor J. T., and Keil K. 1992. Martian parent craters for the SNC meteorites. *Journal of Geophysical Research* 97:10,213–10,225.

Newsom H. E., Hagerty J. J., and Thorsos I. E. 2001. Location and sampling of aqueous and hydrothermal deposits in Martian impact craters. *Astrobiology* 1:78–88.

Osinski G. R. 2006. Effect of volatiles and target lithology on the generation and emplacement of impact crater fill and ejecta deposits on Mars. *Meteoritics & Planetary Science* 41:1571–1586.

Rathbun J. A. and Squyres S. W. 2002. Hydrothermal systems associated with Martian impact craters. *Icarus* 157:362–372.

Scott D. H and Tanaka K. L. 1986. Geologic map of the western equatorial region of Mars, 1:15,000,000. U. S. Geological Survey Miscellaneous Investigation Series Map I-1082-A.

Schultz P. H. 1992. Atmospheric effects on ejecta emplacement. *Journal of Geophysical Research* 97:11,623–11,662.

Schultz P. H. and Gault D. E. 1979. Atmospheric effects on Martian ejecta emplacement. *Journal of Geophysical Research* 84:7669–7687.

Stewart S. T. and Valiant G. J. 2006. Martian subsurface properties and crater formation processes inferred from fresh impact crater geometries. *Meteoritics & Planetary Science* 41:1509–1537.

Strom R. G. and Fielder G. 1971. Multiphase eruptions associated with the craters Tycho and Aristarchus. In *Geology and physics of the Moon; a study of some fundamental problems*, edited by G. Fielder G. Amsterdam, New York: Elsevier. pp. 55–92.

Zuber M. T., Smith D. E., Solomon S. C., Muhleman D. O., Head J. W., Garvin J. B., Abshire J. B., and Bufton J. L. 1992. The Mars Observer Laser Altimeter investigation. *Journal of Geophysical Research* 97:7781–7797.